Estimation of Undrained Strength and Soil Rigidity Index of Clays Using Penetration and Cavity Expansion

Jian Yu[1#], *Junlin Zhu*[1], *Maosong Huang*[1], *Yifeng Lin*[2] and *Zhenhao Shi*[1]

[1] *Tongji University, Department of Geotechnical Engineering, Siping Road 1239, Shanghai 200092, China,*
[2]*Shanghai Investigation Design and Research Institute Co., Ltd., Linxin Road 65, Shanghai 200335, China*
[#]*Corresponding author: 002yujian@tongji.edu.cn*

ABSTRACT

The current cone factor of piezocone penetration tests is derived based on the assumption of elastic-perfectly plastic soil, and the soil rigidity index in the formula is empirically determined. This study introduces a novel in-situ testing equipment for determining both undrained shear strength and soil rigidity index of clays. The presented technique combines cone penetration test (CPT) and in-situ expansion. Indoor experiments are conducted to test the equipment. Corresponding theoretical analysis is carried out to interpret the experimental results. A hyperbolic hardening soil model for undrained clay is used throughout the derivation process so that the nonlinear stress-strain relation is taken into account. The ALE (Arbitrary Lagrangian Eulerian) large deformation finite element method is first employed to analyse the influence factors such as rigidity index, cone roughness, and in-situ stress anisotropy during the penetration process. The formula of cone factor is then proposed and correlated with the limit expanding pressure of the spherical cavity. The rationality of the cone factor is verified by comparing with the ALE analysis results and those published studies. Besides, the limit pressure of in-situ expansion tests is determined based on the load-displacement curve of cylindrical cavity expansion, Specific bearing capacity formula is derived and revised based on finite element analyses. Finally, undrained shear strength and soil rigidity index are solved based on the penetration and expansion results. Interpretation of experimental results shows that the proposed method in conjunction with the newly developed CPT can reasonably predict the undrained strength and rigidity index of soft soils.

Keywords: cone penetration test; finite element analyses; spherical and cylindrical cavity expansion; nonlinear stress strain.

1. Introduction

Cone Penetration Testing (CPT) is extensively utilized for in-situ testing in geotechnical engineering. By measuring continuous parameters such as cone tip resistance, sleeve friction, pore water pressure (CPTU), or shear wave velocity (SCPT), the outcomes can be interpreted to determine strength parameters of clay, assess the bearing capacity of pile foundations, and evaluate the liquefaction potential of sandy soils, etc. Typically, the strength parameters of clay are determined based on the cone tip resistance as follows:

$$s_u = \frac{q_c - \sigma_{v0}}{N_{kt}} \tag{1}$$

Once the cone factor N_{kt} is established, the shear strength value can be obtained. Current research typically treats cone penetration in saturated clays as an undrained problem and uses the elastic-perfectly plastic model to describe the stress-strain characteristics of the soil (e.g. Lu et al., 2004; Liyanapathirana, 2009). Many soil parameters are also derived based on the Cam-Clay model, such as the coefficient of earth pressure at rest (K_0), the overconsolidation ratio (OCR), and the internal friction angle. There are numerous empirical or semi-empirical formulas for these parameters (referencing Mayne, 2001; Robertson, 2009). However, these formulas fundamentally adopt the elastic-perfectly plastic model assumption. They first establish the undrained strength and then build a connection with parameters such as OCR based on the critical state theory.

The elastic-perfectly plastic model, in reality, cannot accurately describe the stress-strain characteristics of soil, which may result in significant errors when determining undrained shear strength. As stated by Salgado et al. (1997) and Tolooiyan and Gavin (2011) in their analyses of cavity expansion problems, soil stress-strain nonlinearity has a noticeable impact on the limit pressure of cavity expansion, thus greatly diminishing the accuracy of the elastic-perfectly plastic model. Therefore, this paper assumes the clay as a hyperbolic elastoplastic model, fully considering the influence of nonlinear stress-strain characteristics on cone factor.

It is widely recognised that cone factor N_{kt} depends on the soil rigidity index for which the latter is unknown in the penetration process and is supposed to be estimated using other techniques, such as in-situ expansion. The existing in-situ testing equipments (e.g. CPT or CPTU) cannot simultaneously measure strength and soil rigidity index, as a result, this study designed a novel testing equipment that combines cone penetration and in-situ expansion in soft clay. To interpret the the newly developed CPT testing technique, a simplified method is

first proposed to determine the cone factor N_{kt} using large deformation finite element methods and spherical cavity expansion techniques. In the meanwhile, the limit pressure of in-situ expansion tesing is founded through the finite element analyses. Consequently, both the undrained shear strength and soil rigidity index are solved based on the penetration and expansion results. Finally, a set of combined testing apparatus developed in-house is employed to carry out indoor model experiments to verify the methods proposed in this study.

2. Simulation of spherical and cylindrical cavity expansions

2.1. Model setup and validation of Cone penetration analysis

Fig. 1 illustrates the finite element mesh for cone penetration simulation. A standard cone with a 60° apex angle and a 36-mm diameter is modelled in an axisymmetric setup. The material property of cone is discrete rigid body, which is composed of a shaft, cone tip and retaining wall. According to the trial calculation, a penetration distance of 20 cone diameters is required, so the soil mass is extended 40 and 25 cone diameters in vertical and radial directions, respectively. This will ensure no boundary effect. The discretization of clay contains a total of 12840 four-node reduced-integration elements (CAX4R). For the boundary condition, the outer and bottom edges are displacement boundaries, while the subsurface is a stress boundary.

Initially, the cone tip is placed below ground in such a way that the grid at ground is less susceptible to distortion. Cone penetration is simulated as a quasi-static process keeping a rate of 2cm/s. Throughout the analysis, the shaft and retaining wall are in smooth contact with the soil. The frcition between cone tip and clay follows Coulomb's law, where a friction coefficient and a limit shear stress $\tau_{\max}$ are introduced to control the interface finite-sliding. It is given by $\tau_{\max} = 2s_u/\sqrt{3}$ as per Liyanapathirana (2009). In visualization, the interaction contact CFT2 of history output requests is obtained as the vertical penetration resistance. The smooth retaining wall is situated at the centre of the mesh to prevent inward movement of clay, and also to minimine piercing distortion at the cone tip.

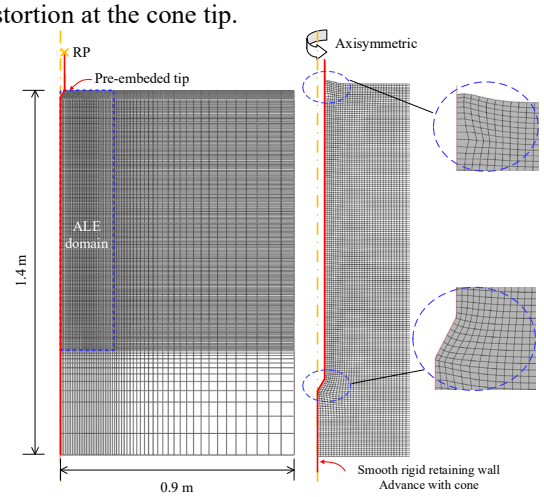

Figure 1. Finite element analysis setup.

To reduce the computational cost, part of the soil region is activated for ALE adaptive meshing, as shown in Fig. 1. Both the mass and time scaling factor are properly set as they affect the computational time. The success of ALE remeshing technique depends more on the remeshing frequency. Therefore, for the results presented in this study, a new mesh is created at the end of each time increment using three sweeps. Griffiths (1982) has already demonstrated the numerical breakdown caused by the Poisson's ratio of soils. With the increase of Poisson's ratio, the computed cone resistance with penetration depth tends to show intense oscillation (Sheng et al., 2013). This is clearly a limitation of Explicit FE analysis. As a result, the undrained penetration would give more obvious oscillation relative to drained analysis. Finally, a uniform Poisson's ratio of 0.49 was chosen for the analyses.

The computed cone tip resistance is shown in Fig. 2, numerical oscillation actually exists but is absolutely acceptable. In Fig. 2, all cone tip resistances rapidly reach a steady state that used to evaluate the cone factor. Additionaly, both s_u and σ_{v0} can be completely normalised using Eq. (1) when keeping constant rigidity index G/s_u. The penetration bearing coefficient for the smooth cone was calculated using the elastic-perfectly plastic model. This was then compared with existing literature to validate the accuracy of the finite element model used in this study. The details of this comparison are not elaborated upon here.

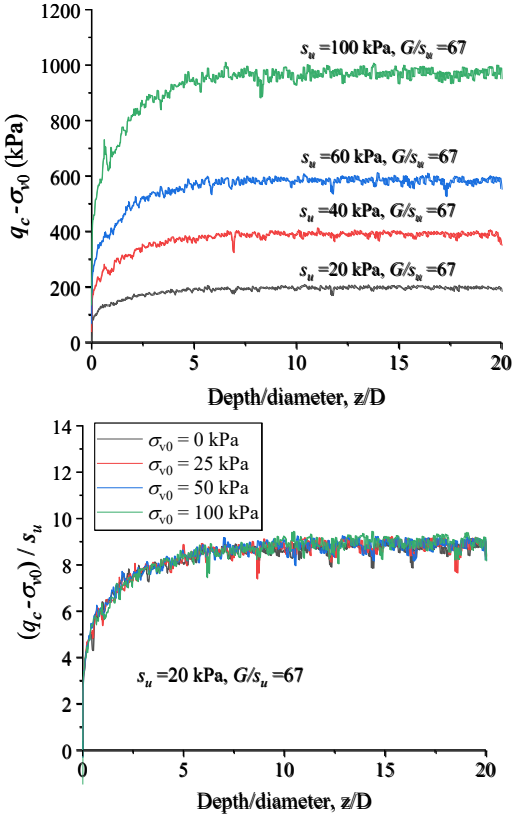

Figure 2. Computed cone tip resistance with penetration depth (varying s_u).

2.2. Cone penetration analysis with a hyperbolic hardening soil model

The saturated soft clay is considered as a purely elastoplastic material with great non-linearity. The soil follows a general hyperbolic hardening,

$$\tau = \frac{\gamma}{\frac{1}{G} + \frac{\gamma}{s_u} R_f} \tag{2}$$

where G is the initial shear modulus, τ is the shear stress, R_f is the failure ratio, γ is the shear strain. From the point of view of simplicity, the hyperbolic hardening model is implemented using built-in Mohr-Coulomb plasticity model in Abaqus. This operation implies an associated flow rule and the isotropic hardening rule as well as the Tresca yield criteria.

Fig. 3 compares the computed cone factors using two different soil model. In the hyperbolic hardeningmodel, the failure ratio is temporarily set to 1.0. It is clear that, under the same initial modulus G, the elastic-perfectly plastic model constantly gives higher cone factors than the other one. The cone tip resistance not only varies with soil rigidity index, but is also affected by the stress-strain non-linearity of the soil. The comparison in Fig. 3 is sufficient to reveal the significance of stress-strain non-linearity in soil. However, previous literature did not focus on and provide relevant arguments.

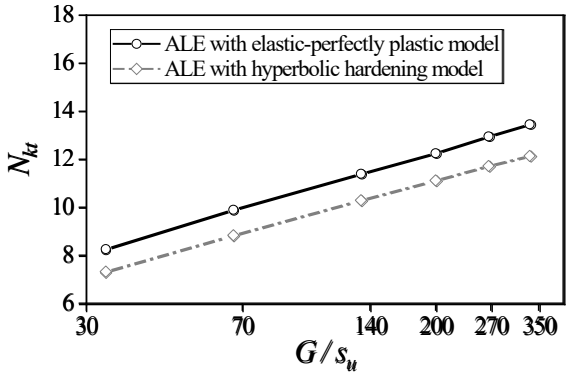

Figure 3. Comparision of cone factor in various soil models.

The interface contact between the cone and soil is an inevitable practical problem. Although it does not provide a great force for cone penetration as in sandy soils, the contribution of the vertical component of interface shear stress to cone factor cannot be ignored. In this study, only cone tip-soil contact is taken into account, since Lu et al. (2004) has shown that the roughness of the shaft does not have any effect on cone factors. When the friction coefficient α_c varies between 0 and 1, cone factors have an approximately linear increase, as shown in Fig. 4. The gradients of the parallel lines with various rigidity indices are about $\sqrt{3}$. In this observation, the interface force is independent of soil models.

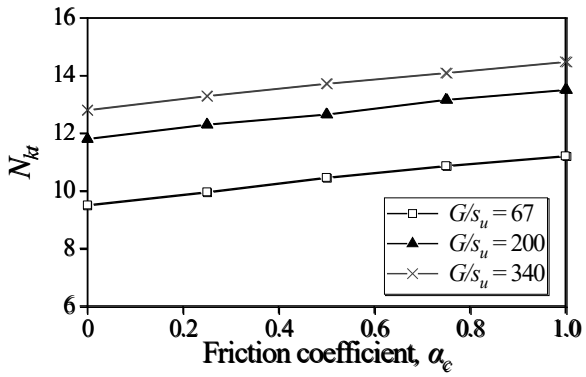

Figure 4. Influence of cone roughness on cone factor.

It has been demonstrated that the in-situ stress within the soil has an important effect on the cone tip resistance. By using the in-situ stress ratio Δ defined by Teh and Houlsby (1991), Yu et al. (2000), Lu et al. (2004), and Liyanapathirana (2009) performed finite element analysis to check the effect of initial stress anisotropy on cone factors. Their analyses gave close influence coefficients of 1.83 , 1.9 and 1.7 for the elastic-perfectly palstic soil. In addition, they noted that the cone factor defined based on the vertical stress is somewhat more sensitive to the in-situ stress ratio than the cone factors defined based on the horizontal σ_{h0} and mean stress p [see Eq. (1)]. However, the vertical stress σ_{v0} was still suggested to calculate the cone factor for the reason that horizontal stress is usually unknown in engineering.

As is widely recognised that the initial stress anisotropy will affect the loading stress path of soils, and this effect is supposed to vary with soil models, i.e. stress strain relations. For this purpose, the discussion on the in-situ stress ratio is presented again using the hyperbolic hardening model. At first, for the elastic-perfectly plastic model, the current analysis obtained an anverage influence coefficient of k=1.9, very consistent with those of Yu et al. (2000), Lu et al. (2004), and Liyanapathirana (2009). It can be seen from Fig. 5 that, the dependence of the influence coefficient on the soil rigidty index. Fig. 5 also demonstrates that the failure ratio R_f has discernible influence on coefficient k. With the decrease of R_f , the influence coefficient of initial stress anisotropy tends to increase, but is still far less than the coefficient of elastic-perfectly plastic model.

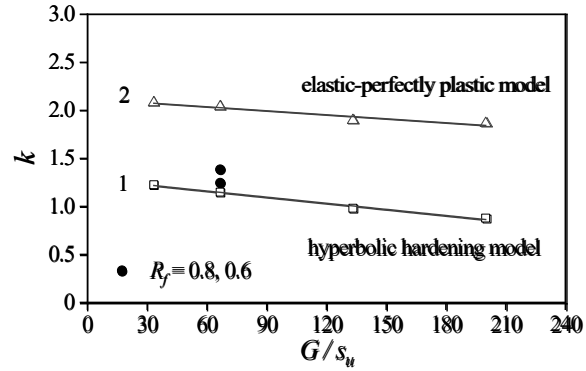

Figure 5. Variation of influence coefficient with soil rigidity index.

2.3. Modified spherical cavity expansion method

In above sections, soil is modelled as a hyperbolic hardening material, and the analyses show the effects of soil rigidity index, cone roughness, initial stress anisotropy and paramter R_f on the cone factor. The final relationship for cone factor may be obtained by combining these terms, to arrive at

$$N_{kt} = f\left(E/s_u, R_f\right) + \sqrt{3}\alpha_c - 1.0\Delta \tag{3}$$

Note that so far in this study, this expression did not give an explicit relation on G/s_u and R_f. Cone roughness is found to be independent of soil stress strain so that its effect can be concluded by fitting the FEA results. For simplicity, the effect of in-situ stress ratio is also evaluated as a constant, though it shows slight correlations with the soil rigidity index and R_f. Consequently, this section mainly pay attention to a smooth cone advancing in isotropic clays. The cavity expansion approach is introduced to compute the cone factor.

The schematic of cone penetration is shown in Fig. 6, the calculation circumference meets the following elliptical function,

$$\frac{\left(r\cos\theta\right)^2}{\left(r_0\right)^2} + \frac{\left(r\sin\theta\right)^2}{\left(\sqrt{3}r_0\right)^2} = 1 \tag{4}$$

where r_0 =D/2, D denotes the cone diameter. r is the calculation radius varying from length OA to OB, the corresponding angle is θ. All radial stresses on the circumference are equal everwhere and point towards the center point-O. As previously noted by Lu et al. (2004) and Liyanapathirana (2009), both radial and vertical extent of the plastic zone around the cone tip is closer to the spherical cavity expansion solution relative to the cylindrical cavity. Therefore, the radial stress equals to the limit expanding pressure of spherical cavity expansion.

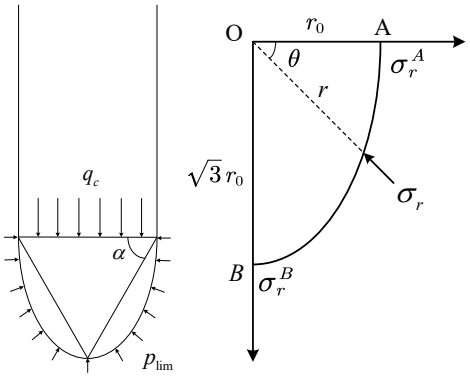

Figure 6. Schematic of soil expansion for cone penetration.

The vertical stress of any point on the circumference A-B is,

$$\sigma_y = \sigma_r \cdot \sin\theta \tag{5}$$

Since there is no interface friction on the cone surface for fully smooth cones, the vertical cone tip resistance q_c is obtained by integrating σ_y along path A-B,

$$q_c = \frac{\int_0^{\frac{\pi}{2}} \sigma_y}{l_{OA}} = \int_0^{\frac{\pi}{2}} \sigma_r \cdot \sin\theta \cdot \sqrt{\frac{3}{2\cos^2\theta + 1}}\, d\theta \tag{6}$$

Equation (6) further results in constant relation q_c = $1.4038 p_{\lim}$. There is a multiple relationship between cone tip ultimate resistance and limit expanding pressure of spherical cavity. It should be noted that σ_r and $p_{\lim}$ in Eq. (6) do not contain the initial stress σ_{v0}. Regardless of the level of initial stress, numerical analyses give identical cone factors (Lu et al., 2004). Consequently, the cone factor N_{kt} is related,

$$N_{kt} = \frac{q_c - \sigma_{v0}}{s_u} = 1.4038 N_s \tag{7}$$

where N_s is the bearing capacity factor of spherical cavity expansion. For the elastic-perfectly plastic clay, N_s becomes

$$N_s = \frac{4}{3}\left[1 + \ln\left(G/s_u\right)\right] \tag{8}$$

Fig. 7 carries out comparison of the cone factor to verify the proposed relation. The spherical cavity factor is obviously far less than the cone factor. The proposed correlation equation [combining Eq. (7) and (8)] gives close estimations of cone factor to finite element results. In the same figure, the theoretical solutions given by Ladanyi and Johnston (1974), Vesic (1977) and Yu et al. (1993) are also plotted. They are all derived in the framework of cavity expansion theory, for elastic-perfectly plastic soils. Fig. 7 indicates the greater ability of the proposed correlation to predict the cone factor. According to the FEA results in Fig. 7, the ratio N_{kt} /N_s does not seem to keep constant with soil rigidity index. Teh and Houlsby (1991) has taken it into account by fitting finite element results, however, the effect is not considered in present study for twofold reasons. Firstly, the limit equilibrium method does not hold the ability to analyze such problem related to soil rigidity index. Moreover, when the stress strain non-linearity is fully considered, the computed ratio N_{kt}/N_s does not show obvious dependence on soil rigidity index anymore (see Fig. 8).

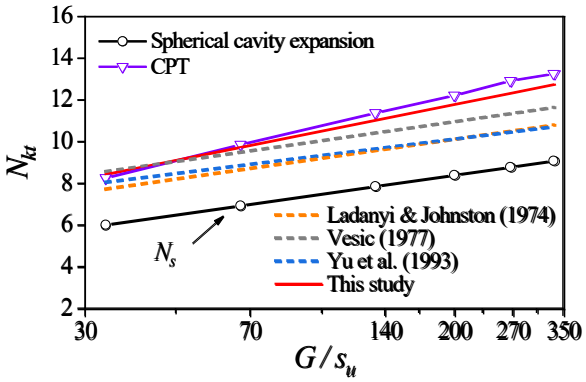

Figure 7. Cone factor comparision for elastic-perfectly plastic soil.

It should be pointed out that, in principle, Eq. (7) is only applicable to elastic-perfectly plastic soils. This is because the limit equilibrium method assumes that the soil in the failure zone is completely plastic, while the soil outside the failure zone is purely elastic, conforming to the assumption of elastic-perfectly plastic model. To

accommodate the hyperbolic hardening soil model, the proposed correlation is modified as,

$$N_{kt} + n_k n_s = 1.4038\left(N_s + n_s\right) \quad (9)$$

where n_k is the ratio of spherical cavity factor N_s to cone factor N_{kt} that determined from finite element analyses, for elastic-perfectly plastic soils. Numerical calculations in this study give an average ratio of n_k =0.7. n_s is the difference of the spherical cavity factor between the elastic-perfectly plastic model and the hyperbolic hardening model. In this conversion, cone factors by various soil models are uniformly related to those by elastic-perfectly plastic model, which is used as the baseline model.

The spherical cavity expansion solution is required for the validation of Eq. (9). Conveniently, this section carries out finite element analyses to determine the spherical cavity factor N_s.

The ultimate bearing capacity coefficient of spherical expansion increases with the increase of the rigidity index G/s_u and decreases with the increase of the failure ratio R_f. Since there is no mutual influence between the rigidity index G/s_u and the failure ratio R_f, and the problem has few parameters with strong regularity, the ultimate bearing capacity coefficient of spherical expansion can be directly deduced from the finite element results, to give

$$N_s = \frac{4}{3}\left[\ln\left(G/s_u\right) - 0.65R_f{}^4 + 0.68\right] \quad (10)$$

This formula is very similar to the plastic analytical solution in elastic-perfectly plastic clays by Gibson and Anderson (1961).

The variation of spherical cavity factor with soil rigidity index is shown in Fig. 8. The difference n_s in Eq. (9) is 1.3 (R_f =1 in the hyperbolic hardening model), showing no variation with soil rigidity index. It is clear that the predicted cone factors using the modified correlation agree well with the FEA results.

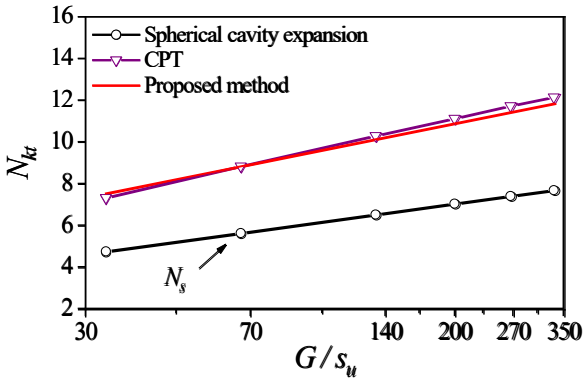

Figure 8. Cone factor comparison for hyperbolic hardening soil.

2.4. Modified cylindrical cavity expansion method

Referring to the spherical expansion bearing capacity coefficient given in Eq. (10), using the hyperbolic hardening model, the bearing capacity coefficient N_c for the cylindrical cavity expansion can be obtained as follows:

$$N_c = \ln\left(G/s_u\right) - 0.65R_f{}^4 + 0.68 \quad (11)$$

This formula is derived based on the plane strain condition. However, current studies have indicated that the effect of a cavity with finite length on the ultimate expansion force is significant. Therefore, further numerical simulations on lateral pressure loading for different aspect ratios are conducted in order to consider revisions to the limit expansion pressure.

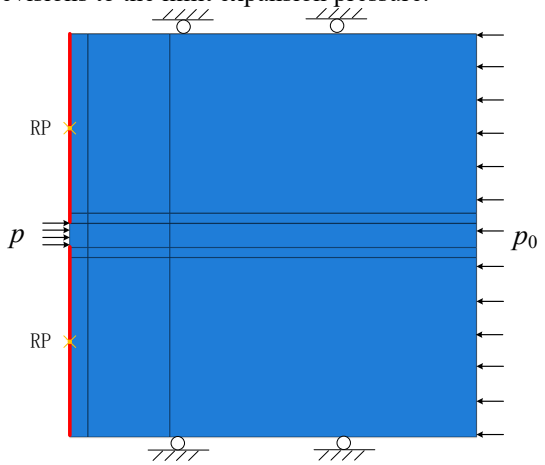

Figure 9. 3D finite element setup.

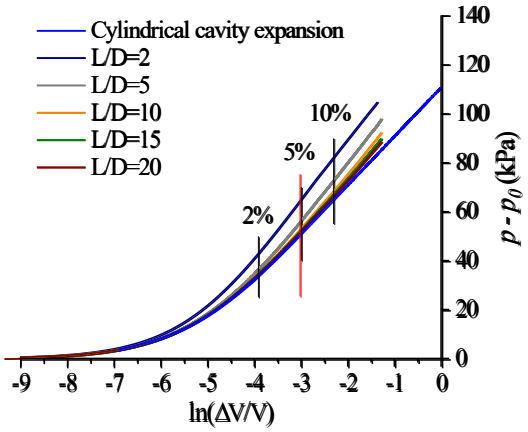

Figure 10. Expansion curves with various L/D (G/s_u =200, R_f =0.9).

An axisymmetric finite element model is constructed with a computational domain in the vertical and radial directions of $200a_0$, as illustrated in Fig. 9. The initial radius of the cavity is a_0, and the mesh is densified within the $5a_0$ range above and below the expansion segment. A uniformly distributed pressure p_0 is applied to the right boundary to simulate isotropic initial stress conditions. The vertical displacement of the upper and lower boundaries is constrained, and the setup includes a fixed rigid body in smooth contact with the left side of the soil. The length of the expansion segment is L, and numerical simulations are conducted for different aspect ratios (L/D) by applying a uniform loading pressure p.

Employing a hyperbolic hardening model, the computation is conducted for undrained total stress analysis. The maximum loading stress value is to ensure a/a_0=1.2, which means that the volumetric strain of the cavity reaches 30%. Fig. 10 illustrates the p- $\ln\left(\Delta V/V\right)$ expansion curves, where $\Delta V/V$ is defined as $\left(a^2 - a_0{}^2\right)/a^2$, and p_0=100 kPa.

Further calculations were performed for eight combinations of parameters G/s_u and R_f with aspect ratios L/D of 2, 5, 10, 15, and 20, totaling 40 cases. The influence on the limit expansion pressure can be concluded as:

$$\beta = p_{\lim}^{L/D} / p_{\lim}^{\infty}$$
$$\beta = 1.307 - 0.09 \cdot \ln(L/D) \quad (12)$$

where $p_{\lim}^{L/D}$ and $p_{\lim}^{\infty}$ respectively correspond to the ultimate expansion pressures determined under finite L/D size conditions and plane strain conditions.

3. Penetration and Expansion Joint Test

The 1g physical model experiment has the advantages of low testing cost, strong controllability, simple operation and processing, and strong repeatability. This study developed a cone penetration-expansion combined testing device, as shown in Fig. 11, to demonstrate how the strength and stiffness of saturated clays can be calibrated through combined cone penetration test (CPT) and expansion testing. As the probe is currently in the prototyping stage, its diameter is larger than the standard probe, measuring 7 cm, and includes an expansion segment of 14 cm.

Malaysian kaolin was used in the experiments, and its physical and mechanical properties can be obtained from Purwana (2007) as shown in Table 1. The use of standard clay is advantageous for generalizing conclusions and improving the success rate of the experiment due to its clear mechanical properties.

Table 1. Properties of Malaysian Kaolin clay (Purwana, 2007)

Parameters	**Value**
Unit weight,γ (kN/m^3)	16.4
Liquid limit (%)	80
Plastic limit (%)	35
Internal friction angle of internal, φ(deg)	23~25
Coefficient of permeability, k (m/s)	2.0×10^{-8} (100 kPa)
Coefficient of consolidation, c_v(cm^2/s)	4.76×10^{-5} (12.5-100 kPa) 7.62×10^{-5} (200-800 kPa)
Critical state friction constant, M	0.9
Gradient of normal consolidation line, λ	0.244
Gradient of swelling line, κ	0.053
Specific volume at p'=1kPa, N	3.35
Strength ratio, $(s_u/\sigma_{v0})_{NC}$	0.22 (Yu et al., 2017)

Firstly, using the designed automatic pressure control consolidation device, the remolded saturated slurry is consolidated under K_0 conditions at the state of 100 kg to prepare the saturated soil layer. During the experiment, the vertical confining stress is maintained simultaneously to simulate the effective stress level in the earth's strata. This experiment studies the in-situ calibration methods for the undrained shear strength and the rigidity index. While conducting the cone penetration and in-situ expansion tests, T-bar penetration tests are also carried out to clarify the strength distribution of the soil layers.

(a)

(b)

(c)

Figure 11. Penetration and Expansion Joint Test: (a) Model Probe; (b) Model set-up; (c) Test photo.

Fig. 12 presents the shear strength profile obtained using the T-bar test, where a value of $N_{T\text{-}bar}$ =10.5 is used for converting to s_u. The designation T100 indicates that the vertical consolidation pressure on the soil surface is 100 kg, with two pressure cylinders amounting to 200 kg (equivalent to a surface vertical pressure of 5.87 kPa).

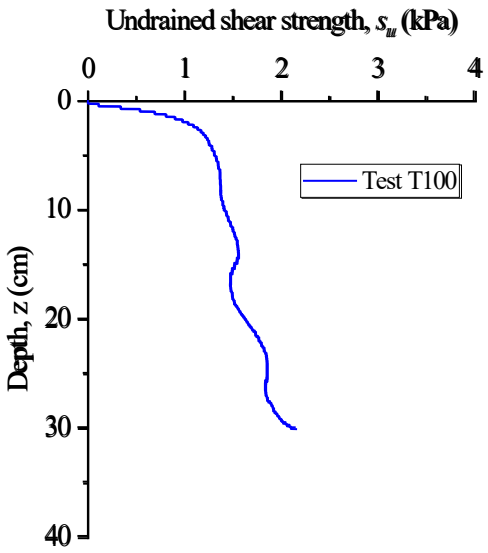

Figure 12. Undrained strength profile from T-bar test.

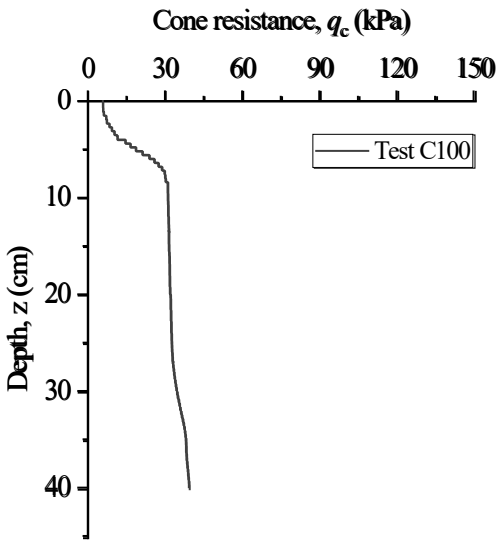

Figure 13. Cone tip resistance along depth.

Fig. 13 illustrates the cone tip resistance measured during the penetration process, while Fig. 14 presents the load-displacement curve obtained from expansion tests conducted after the cessation of penetration, which is plotted on a p- $\ln(\Delta V/V)$ diagram. Taking the test results presented in Figs. 13 and 14 as an example, this section explains how to determine the undrained strength and rigidity index based on the results of cone penetration and expansion tests.

A distinct linear segment is observed in Fig. 14, which has been fitted using the method of least squares to ascertain that the intercept of this linear portion with the vertical axis, corresponding to the limit expansion pressure, which equals 21.35 kPa. After deducting the initial stress p_0 at the current depth, the limit expansion pressure $p_{\lim}$ is evaluated to be 14.2 kPa. In this test, the expansion apparatus has an aspect ratio (L/D) of 2, and taking into account the correction for geometric dimensions as per Eq. (12), the correction coefficient β for the limit expansion pressure is determined to be 1.2526. Consequently, the value of the limit expansion pressure $p_{\lim}$ is adjusted to 11.33 kPa.

The expansion test is conducted at a depth of z = 20 cm where the cone tip penetration resistance is measured to be 32.08 kPa. Using Eq. (9) for the cone factor, n_k=0.7, the value of n_k is determined as the difference obtained by subtracting Eq. (10) from Eq. (8). Assuming a failure ratio R_f of 0.9 and utilizing the cylindrical cavity expansion Eq. (11), we can get

$$N_{kt} = \frac{q_c - \sigma_{v0}}{s_u} = \frac{4}{3} \times 1.4038 \times \left[1 + \ln\left(G/s_u\right)\right] + 0.086$$
$$N_c = \frac{p_{\lim}}{s_u} = \ln\left(G/s_u\right) + 1.0921 \quad (13)$$

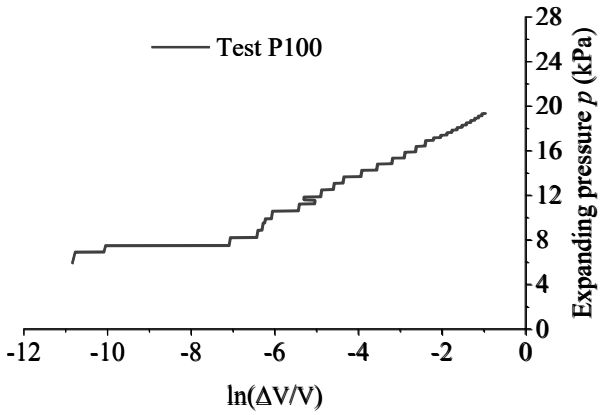

Figure 14. Expanding curve in Malaysian kaolin clay.

Incorporating the cone roughness coefficient into the cone factor, Lu et al. (2004) indicates that the in-situ cone tip roughness coefficient typically ranges between 0.2 to 0.6; in this study, it is taken as 0.4. Solving Eq. (13) yields an undrained shear strength (s_u) of 2.1162 kPa and a rigidity index (G/s_u) of 275.35. This strength value is slightly greater than the results from the T-bar test shown in Fig. 12. Based on the triaxial undrained shear tests as reported by Banerjee and Malek (2020), Ho (2013), and Duque et al. (2022), the range of ε_{50} for the Malaysian kaolinite was determined to be within 0.0025 to 0.0033. ε_{50} (= s_u/E_{50} , E=3G=2E_{50}/(2-R_f)) measured in this study is 0.0022, which is close to the existing results. The final calculated cone factor N_{kt} is 13.166.

4. Conclusions

Existing numerical or analytical analyses typically assume that saturated clays behave as elastic-perfectly plastic materials, overlooking the influence of stress-strain nonlinearity on CPT penetration. Moreover, a notional soil rigidity index is often used to evaluate the cone factor, resulting in calculation errors in shear strength. From this perspective, the present study enhances the in-situ testing methods for soil strength and rigidity index. The newly developed CPT equipment has a shaft that can expand. Indoor model tests including

cone penetration and subsequent in-situ expansion in saturated clay were then conducted.

To interpret the test results, a set of analysis method is carried out. The stress-strain nonlinearity is taken into account throughout the analyses. Initially, cone penetration test is simulated with the aid of large deformation finite element, investigating the relationship between the cone factor and influence factors such as the cone surface roughness, in-situ stress ratio, and soil rigidity index. A cone tip resistance evaluation method based on spherical cavity expansion limit pressure is then established, which can accurately calculate the cone factor considering soil nonlinearity. Subsequently, the limit pressure of in-situ expansion testing is derived within cylindrical cavity expansion theory and modified through 3D finite element expansion. Finally, a combination of cone tip penetration resistance and in-situ expansion limit pressure is utilized to solve jointly for the undrained shear strength and rigidity index.

Compared with indoor experimental results, the interpretion method accurately calculates the undrained shear strength and soil rigidity index. The theory and testing equipment in this study require further improvement, but based on this research, it is suggested that the influences of soil stress-strain nonlinearity should be considered in the cone penetration analysis of saturated clays, and soil rigidity index should be carefully determined, which would contribute to enhancing the accuracy of in-situ undrained shear strength evaluations.

Acknowledgements

This work was financially supported by the National Natural Science Foundation of China (Grant Nos. 51908420) and the Research Project of China Three Gorges Corporation Limited (Grant Nos. 202103495). These supports are gratefully acknowledged.

References

Banerjee, S., Malek, S., 2020. Assessment of a hyperbolic model for undrained-cyclic shearing of remolded clay. *J. Eng. Mech*. 146 (7), 04020064.

Duque, J., Roháč, J., Mašín, D., Najser, J., 2022. Experimental investigation on Malaysian kaolin under monotonic and cyclic loading: inspection of undrained Miner's rule and drained cyclic preloading. *Acta Geotechnica*. 17(11), 4953-4975.

Gibson R E, Anderson W F., 1961. In-situ measurement of soil properities with the pressuremeter. *Civil Engineering Public Works Reviews*. 56:615-618.

Griffiths, D. V., 1982. Elasto-plastic analyses of deep foundations in cohesive soil. *International Journal for Numerical and Analytical Methods in Geomechanics*. 6(2): 211-218.

Ho, J., 2013. Cyclic and post-cyclic behaviour of soft clays. Nationatioal University of Singapore. PhD thesis.

Ladanyi, B., Johnston, G., H., 1974. Behavior of circular footings and plate anchors embedded in permafrost. *Canadian Geotechnical Journal*. 11(4): 531-553.

Liyanapathirana, D. S., 2009. Arbitrary Lagrangian Eulerian based finite element analysis of cone penetration in soft clay. *Computers and Geotechnics*. 36(5):851-860.

Lu, Q., Randolph, M. F., Hu, Y., Bugarski, I. C., 2004. A numerical study of cone penetration in clay. *Géotechnique*. 54(4):257–67.

Mayne, P. W., 2001. Stress-strain-strength-flow parameters from enhanced in-situ tests. In: Proceedings International Conference on In Situ Measurement of Soil Properties and Case Histories, Bali. 27-47.

Purwana, O.A., 2007. Centrifuge model study on spudcan extraction in soft clay. National University of Singapore. PhD thesis.

Robertson, P. K., 2009. Interpretation of cone penetration tests—a unified approach. *Canadian Geotechnical Journal*. 46(11): 1337-1355.

Salgado, R., Mitchell, J. K., Jamiolkowski, M., 1997. Cavity expansion and penetration resistance in sand. *Journal of Geotechnical and Geoenvironmental Engineering*. 123(4).

Sheng, D., Cui, L., Ansari, Y., 2013. Interpretation of cone factor in undrained soils via full-penetration finite-element analysis. *Int. J. Geomech*. 13(6): 745-753.

Teh, C. I., Houlsby, G. T., 1991. An analytical study of the cone penetration test in clay. *Geotechnique.* 41(1): 17-34.

Tolooiyan, A., Gavin, K., 2011. Modelling the cone penetration test in sand using cavity expansion and arbitrary Lagrangian Eulerian finite element methods. *Computers and Geotechnics*. 38(4): 482-490.

Vesic, A. S., 1977. "*Design of pile foundations*." Nat. Cooperation Hwy. Res. Program Rep. No. 42, Transportation Research Board. Washington, D.C.

Yu H S, Herrmann L R, Boulanger R W, 2000. Analysis of steady cone penetration in clay. *Journal of Geotechnical and Geoenvironmental Engineering*. 126(7): 594-605.

Yu, H. S., Houlsby, G. T., Burd, H. J., 1993. A novel isoparametric finite element displacement formulation for axisymmetric analysis of nearly incompressible materials. *International Journal for Numerical Methods in Engineering*. 36(14): 2453-2472.